ELSEVIER

Journal of Nuclear Materials 251 (1997) 188–199

journal of nuclear materials

The consequences of helium production on microstructural development and deformation response in isotopically tailored ferritic alloys

D.S. Gelles [a,*], G.L. Hankin [b], M.L. Hamilton [a]

[a] *Pacific Northwest National Laboratory, PO Box 999, Richland, WA 99352, USA*
[b] *I.P.T.M.E., Loughborough University, Loughborough, Leicester LE11 3TU, UK*

Abstract

A series of alloys have been made adding various isotopes of nickel to a ferritic/martensitic steel in order to vary the production of helium during irradiation. 1.5% nickel was added to Fe–12Cr either in the form of ^{60}Ni which produces no helium, ^{59}Ni which produces helium at a rate of about 10 appm He/dpa, or natural nickel which provides an intermediate level of helium due to delayed development of ^{59}Ni. Specimens were irradiated in the HFIR to 7 dpa at 300, 400, 500, and 600°C. This paper reports on microstructural differences and differences in deformation response, measured by shear punch testing, found between these specimens irradiated under identical conditions but with the different nickel isotopes. Little microstructural difference was found between specimens with ^{59}Ni and ^{Nat}Ni. Helium bubble development for high helium generation conditions appeared to be very different at 300 and 400°C. At 300°C, it appeared that high densities of bubble-like features formed whereas at 400°C, only voids could be found. The addition of nickel at any isotopic balance to the Fe–12Cr base alloy significantly increased the shear yield and maximum strengths of the alloys with the strength of the alloys decreasing with increasing irradiation temperature. However, helium itself, up to 75 appm at over 7 dpa, appears to have little effect on the mechanical properties of the alloys. © 1997 Elsevier Science B.V.

1. Introduction

Ferritic/martensitic steels are being considered for use as structural materials in fusion reactor systems. In that application, they must not only withstand radiation damage, but also accommodate helium, a transmutation product, to levels as high as several thousand parts per million by end of life. The issue of helium accumulation on properties has been an ongoing concern, but lacking a high energy neutron source capable of high dose, design of unambiguous experiments to study such effects is very difficult.

In order to better understand the effects of helium on embrittlement in ferritic/martensitic steels, an isotopic tailoring [1,2] approach has been taken, similar to that used to study this behavior in austenitic steels [3–5] but requiring irradiation in the high flux isotope reactor (HFIR) or a reactor with similar neutron spectrum. A series of alloys has been made adding various isotopes of nickel in order to vary the production of helium during irradiation by the two step nuclear reaction in a mixed spectrum reactor. The alloys use a base composition of Fe–12Cr with an addition of 1.5% nickel, either in the form of ^{60}Ni which produces no helium, ^{59}Ni which produces helium at a rate of about 10 appm He/dpa, or natural nickel which provides an intermediate level of helium due to delayed development of ^{59}Ni. Although the experiment was first envisioned over ten years ago, specimens have only recently been successfully irradiated in the HFIR at Oak Ridge, TN to about 10 dpa at 300, 400, 500 and 600°C, and examined. This paper reports on two phases of the work involving these specimens: microstructural differences found between these specimens irradiated under identical conditions but with the different nickel isotopes following irradiation at 300 and 400°C and mechanical property response as a function

* Corresponding author. Tel.: +1-509 376 3141; fax: +1-509 376 0418; e-mail: ds_gelles@pnl.gov.

PII S0022-3115(97)00222-5

of helium production based on shear punch testing following irradiation at 300, 400, 500 and 600°C. Given the complexity of the microstructures found, the mechanical properties will first be described, and then the microstructural details will be reported.

2. Experimental procedure

The starting base material for this study, Fe–12Cr bar stock, was obtained from the International Nickel Company, Sterling Forest, NY. Details of alloy fabrication and composition have been published previously [6,7]. The sources of nickel were: ^{60}Ni (batch S-00039) from Oak Ridge National Laboratory supplies, provided by P.J. Maziasz, ^{59}Ni remaining from previous alloy production as described in reference [8] and natural nickel from our laboratory supplies. The ^{59}Ni stock is expected to actually contain only 2.3% ^{59}Ni [8]. The bar stock was pulverized by deformation at low temperature, the required measures of nickel were weighed out to provide 50 g heats, and alloys were melted in a standard arc melting furnace using standard procedures. Losses were found to be negligible. Compositions for the non-radioactive arc melted heats were determined by the Oregon Metallurgical Corporation, Albany, OR and alloy compositions are summarized in Table 1. Alloys were then rolled into 0.20 mm thick sheet. Disks 3 mm in diameter were punched from the sheet, engraved with the unique four digit codes listed in Table 1, and given a heat treatment to duplicate that used in previous fast reactor irradiation experiments (1040°C/1 h/air cool +760°C/1 h/air cool) [6,7,9–11].

Specimens were irradiated in at least a multiplicity of five in the HFIR-MFE-JP23 capsule irradiation located in the G6 target position of HFIR starting December 16, 1993 in cycle 22 and ending June 3, 1994 during cycle 26 for 110.2 effective full power days [12]. The resulting fluences, taking into account specimen positions in reactor, are 3.45×10^{22}, 3.93×10^{22}, 4.21×10^{22}, and 4.37×10^{22} n/cm^2 for the 300, 400, 500 and 600°C conditions, respectively [13]. Table 1 includes estimates of dose and helium accumulation based on reference [13]. Note that significantly more helium is accumulated in specimens containing ^{59}Ni, less for ^{Nat}Ni and negligible amounts for ^{60}Ni and no nickel, whereas only slight further increases in dose arise in ^{59}Ni- and ^{Nat}Ni-containing conditions. Identical specimens at a multiplicity of one were also included in HFIR-MFE-JP-12, -13, -14, -15, and -16 to provide specimens irradiated to 20, 40 and 70 dpa, but those specimens are not yet available for examination.

With the exception of one set of irradiated aluminum alloys [14], shear punch testing has thus far only been carried out on unirradiated materials. A new test facility was set up and a detailed procedure was written to accommodate the shear punch testing of highly radioactive specimens such as these. All tests were conducted under ambient conditions and the results of each test were recorded by computer and simultaneously recorded on a chart recorder.

Shear punch testing is essentially a blanking operation which is common to sheet metal forming. A 1 mm diameter punch is driven at a constant rate of 0.127 mm/min (0.005 in./min) through a TEM-sized disk (nominally 0.25 mm thick and 2.8 mm in diameter). The load on the punch is measured as a function of punch travel, which is

Table 1
Alloy details with heat number, nominal composition, analyzed composition (in wt%), and irradiation conditions (including irradiation temperature, dose in dpa and helium production in appm, and specimen identification codes. All impurities not listed are ≤ 0.01 w/o

Heat #	Nominal	Cr	Ni	C	Other	Irradiation[a]	Code
E62	Fe–12Cr	11.6	na	0.002	$0.026O_2$	300C/6.5dpa/2.1He	6A5 M
						400C/7.3dpa/2.4He	6A5 N
						500C/7.9dpa/2.6He	6A5 O
						600C/8.2dpa/2.7He	6A5 P
R168	Fe–12Cr–1.5^{60}Ni	11.7	1.32	0.004	0.02Si, 0.02Mn	300C/6.4dpa/2.1He	715 M
						400C/7.2dpa/2.3He	715 N
						500C/7.8dpa/2.5He	715 O
						600C/8.1dpa/2.6He	715 P
R169	Fe–12Cr–1.5^{59}Ni	na	na	na	na	300C/6.6dpa/70He	735 M
						400C/7.5dpa/76He	735 N
						500C/8.0dpa/82He	735 O
						600C/8.3dpa/86He	735 P
R170	Fe–12Cr–1.5^{Nat}Ni	11.5	1.54	0.004	0.02Si, 0.02Mn	300C/6.5dpa/41He	745 M
						400C/7.4dpa/46He	745 N
						500C/7.9dpa/50He	745 O
						600C/8.2dpa/51He	745 P

[a] Irradiation temperature/dose/helium production in appm.
na: not available.

taken to be equivalent to the cross head displacement [15]. This assumes that the test machine and punch are completely stiff relative to the response of the test specimen. A plot of punch load versus punch displacement was obtained for each specimen.

The curve obtained from a shear punch test is of a similar form to that obtained from a tensile test. Initially a linear relationship exists between load and punch displacement during which no plastic deformation occurs. This is followed by a deviation from linearity or yield point when permanent penetration of the punch into the specimen occurs. Beyond the yield point, further deformation forms a shear process zone between the die and punch. Work hardening compensates for thinning until a maximum load is achieved [15]. The points of interest on the curve were the yield load and maximum load. Effective shear yield strength (τ_{sy}) and an effective maximum shear strength (τ_{sm}) can be evaluated from these values, respectively, by the following equation [14]:

$$\tau_{sy,sm} = P/(2\pi rt),$$

where P is the appropriate load, r is the average of bore and punch radii and t is the specimen thickness. Previous work has shown that an empirical relationship can be developed between data from shear punch testing and that from tensile testing [14,16,17]. In this instance, however, no tensile data were available and the shear punch test was used only as a tool to identify trends in the mechanical properties that might occur as a result of differing helium levels.

Microstructural examinations are based on specimens prepared as thin foils and extraction replicas using standard techniques. Examinations were performed on a JEOL 1200EX transmission electron microscope operating at 120 keV. As usual, examination required microscope realignment after all routine tilt operations, including condenser and objective lens restigmation and voltage centering. Burgers vector analysis procedures have been previously defined in Ref. [9].

3. Results

3.1. Mechanical properties

At least two tests were performed for each specimen condition listed in Table 1. Reproducibility was good: effective shear strength typically varied by no more than 30 MPa between duplicate specimens. Fig. 1 shows a summary of τ_{sy} as a function of helium content. Fig. 2 shows a similar plot for τ_{sm}. In each case, data for the unirradiated material is included for comparison and alloy conditions containing no intentional additions of nickel are indicated by open symbols.

From the plots of τ_{sy} and τ_{sm}, it can be shown that the addition of nickel to the Fe–12Cr base alloy significantly increases the strength of both the unirradiated and the irradiated alloys, especially for irradiation temperatures of 300 and 400°C. The yield and maximum shear strengths are increased by about 100% compared to the unirradiated

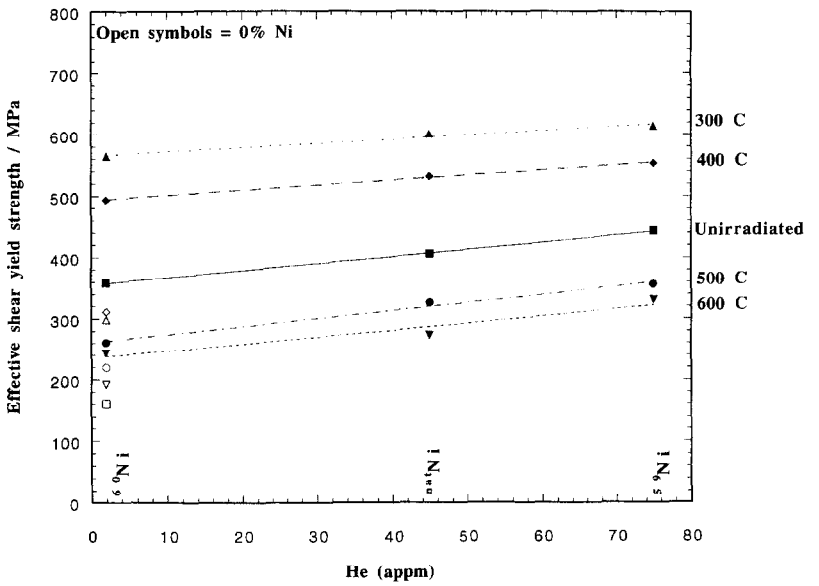

Fig. 1. Effective shear yield strengths (τ_{sy}) in Fe–12Cr–1.5Ni as a function of helium content (an open symbol signifies the control alloy [Fe–12Cr] at the same condition as the corresponding filled symbol).

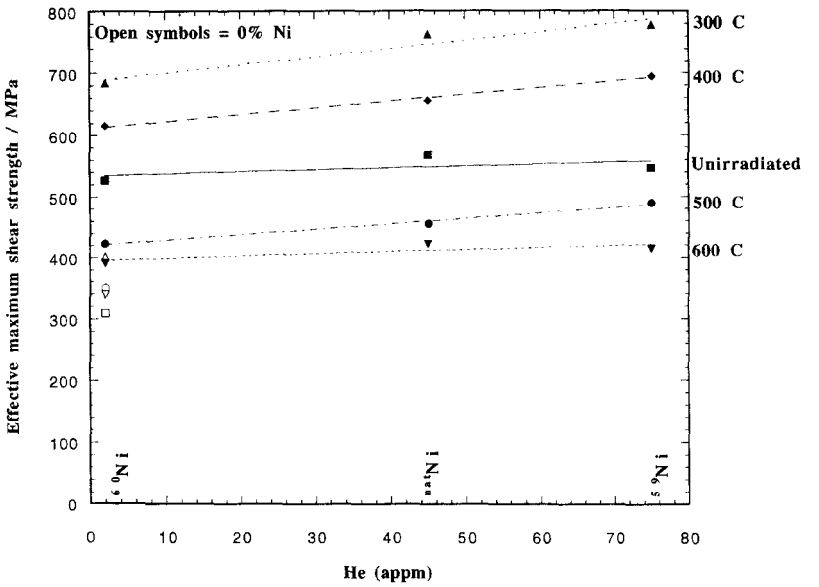

Fig. 2. Effective maximum shear strengths (τ_{sm}) in Fe–12Cr–1.5Ni as a function of helium content (an open symbol signifies the control alloy [Fe–12Cr] at the same condition as the corresponding full symbol).

condition, a result which is independent of the nickel isotope balance used.

In general, the strength of all alloys decreased with increasing irradiation temperature so that the highest strength was observed for alloys irradiated at 300°C. Alloys irradiated at 500 and 600°C actually experienced an overall decrease in strength when compared to the unirradiated condition. However, for the Fe–12Cr material with no nickel added, strengths were similar following irradiation at 300 and 400°C.

A small increase in both τ_{sy} and τ_{sm} can be seen with increasing helium content in the irradiated alloys. Since the same trend is echoed in the data for the unirradiated material, however, it cannot be attributed to the helium level, but rather to another factor inherent to the alloys. Figs. 3 and 4 show the change in τ_{sy} and τ_{sm} with respect

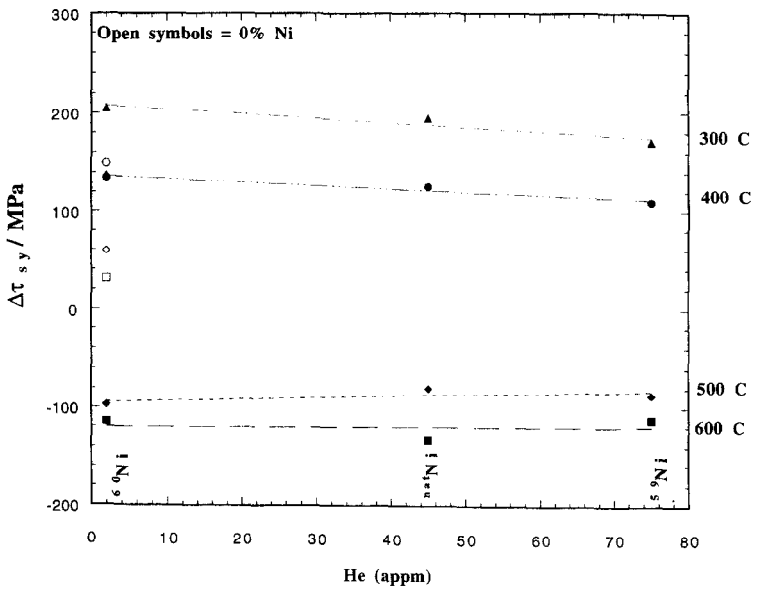

Fig. 3. Change in τ_{sy} with respect to the unirradiated condition as a function of helium content.

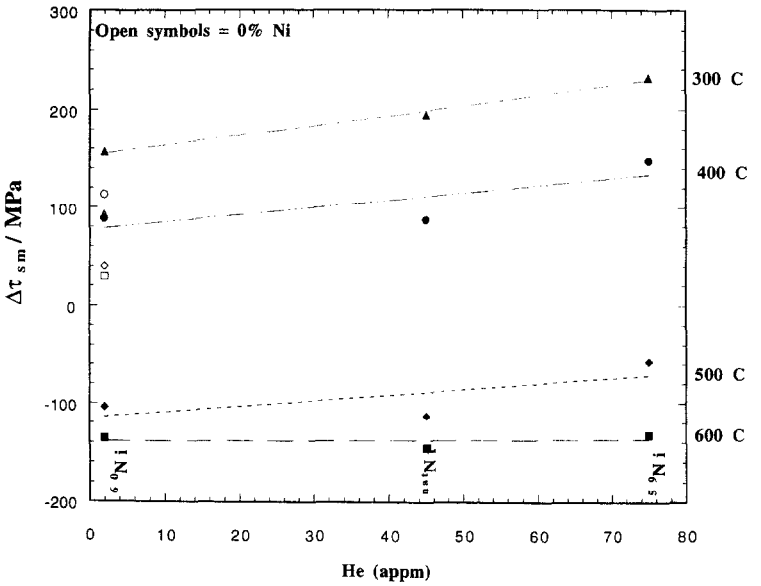

Fig. 4. Change in τ_{sm} with respect to the unirradiated condition as a function of helium content.

to the unirradiated condition ($\Delta\tau_{sy}$ and $\Delta\tau_{sm}$ respectively) versus helium content for each irradiation temperature. While a shallow negative gradient is exhibited at the lower irradiation temperatures for $\Delta\tau_{sy}$, the trend is reversed in Fig. 4 for $\Delta\tau_{sm}$.

3.2. Microstructures

Microstructural damage resulting from irradiation in HFIR was only on a fine scale. Fig. 5 shows low magnification examples of damage at 300 and 400°C respectively for each of the four alloys. The scale of the damage is seen as a fine background mottle. However, the mottling in specimens irradiated at 400°C is coarser than that from 300°C, and the alloy without nickel at 400°C contains mottling that is equiaxed whereas the mottling in the alloys containing nickel is non-equiaxed. Larger particles, for example those in specimen 6A5N, are probably carbides, believed to have been present prior to irradiation.

As the damage is more easily understood following irradiation at the higher temperature, the microstructures formed at 400°C will first be describe in greater detail.

The microstructure of specimen 6A5N, Fe–12Cr, following irradiation to 7 dpa at 400°C and 2 appm He was found to be typical of irradiated Fe–12Cr, and contained dislocation loops, voids and precipitation typical of α', a chromium rich body centered cubic phase often formed by phase separation [18].

An example is provided in Fig. 6, comparing the same area of a specimen in $\vec{g} = 110$ contrast (a), $\vec{g} = 002$ contrast (b) and void contrast (c) for a foil near a $(\bar{1}10)$ orientation. In dislocation contrast, straight dislocations can be identified at the upper left and diagonally across the center from lower left to upper right. Also, many small black spot features can be identified representing small loops in the range 5 to 15 nm in diameter. Comparison of the two dislocation images indicates that more are present under 110 contrast, indicating the loops are generally of Burgers vector $(\frac{a}{2})\langle 111\rangle$. In Fig. 6c, a number of cavities can be identified, as large as 16 nm, but with many as small as 3 nm. Of particular note is the row of three voids of intermediate size in the center that can be show to be connected to dislocations by comparison with the micrographs in dislocation contrast. This area was selected because it contained larger voids, presumably arising from dislocations present prior to irradiation. However, more areas could be found without such dislocations, where only voids on the order of 3 nm were present. Also, in Fig. 6c, a background mottling can be identified that results from α' precipitation. This morphology is typical of the α' phase, with many equiaxed particles, but containing rows of particles in regions containing straight dislocations. This microstructural response to irradiation in HFIR was similar to that found following irradiation in fast reactors, but at a lower dose.

The microstructure of specimen 715N, Fe–12Cr–1.5^{60}Ni, following irradiation to 7 dpa at 400°C and 2 appm He was found to be similar in some ways to irradiated Fe–12Cr, and contained dislocation loops, voids and precipitation typical of α', but loop development was significantly further advanced, examples of larger voids were not found, and precipitate in a rod morphology had developed. Examples are found in Fig. 7. Again, the same area of a specimen can be compared in $\vec{g} = 110$ contrast

(a), $\vec{g} = 002$ contrast (b) and void contrast (c) for a foil near a $(\bar{1}10)$ orientation. Many examples of loops as large as 300 nm can be seen in dislocation contrast. More loops are found under 002 contrast, but several examples can be found only under 110 contrast, indicating that both $a\langle 100\rangle$ and $(\frac{a}{2})\langle 111\rangle$ Burgers vector are present. Again straight dislocation line segments can easily be identified, believed to have been present prior to irradiation. Voids can be identified in Fig. 7c, ranging in size from 3 to 7 nm, but none were found as large as those in specimen 6A5N.

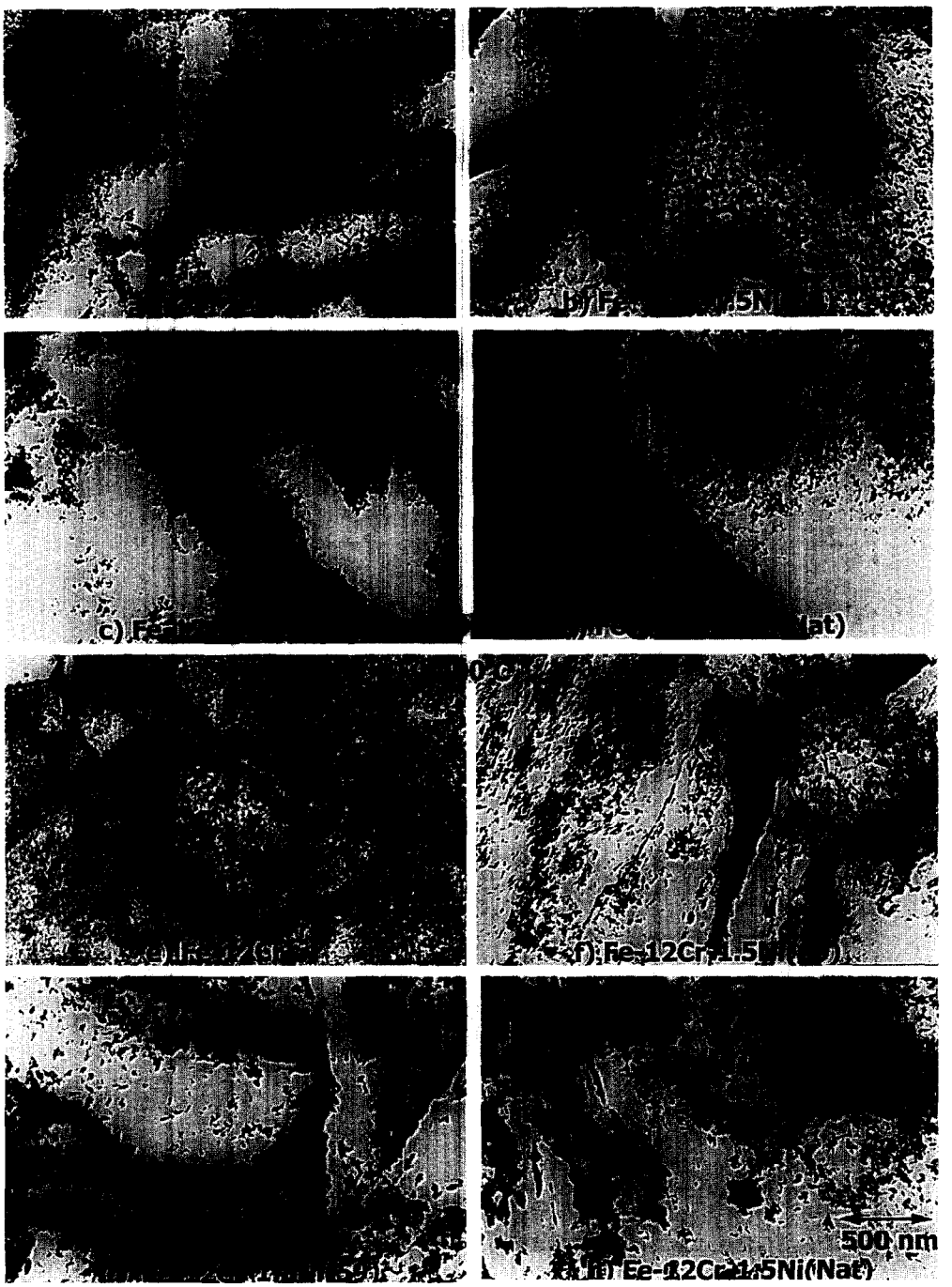

Fig. 5. Microstructures in isotopically tailored Fe–12Cr alloys irradiated at 300 and 400°C to 7 dpa at low magnification.

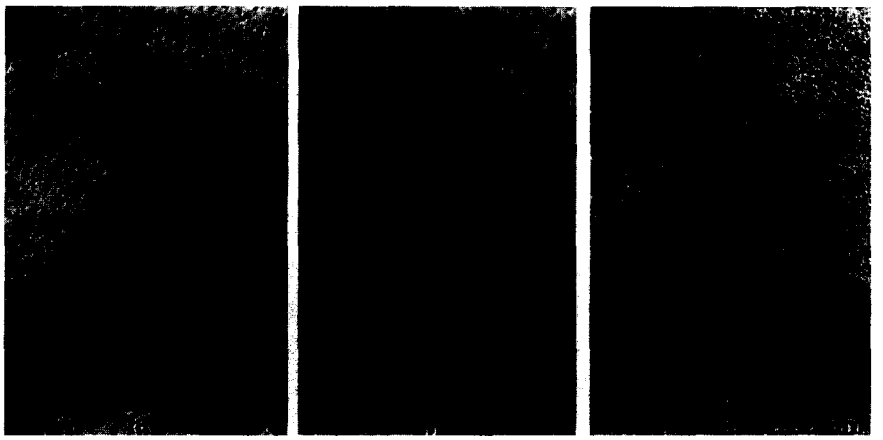

Fig. 6. Fe–12Cr specimen 6A5N irradiated at 400°C to 7.3 dpa and 2 appm He imaged using $\vec{g} = 110$ in (a), $\vec{g} = 002$ in (b) and void contrast in (c) for a foil near (-110) orientation.

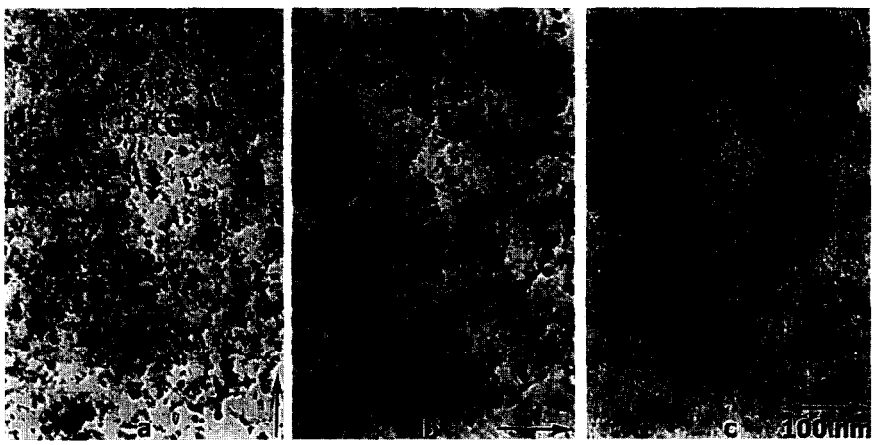

Fig. 7. Fe–12Cr–1.5^{60}Ni specimen 715N irradiated at 400°C to 7.2 dpa and 2 appm He imaged using $\vec{g} = 110$ in (a), $\vec{g} = 002$ in (b) and void contrast in (c) for a foil near $(\bar{1}10)$ orientation.

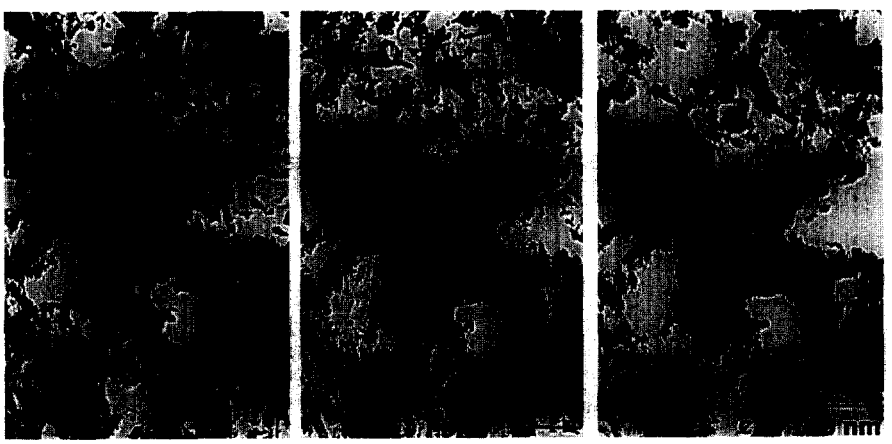

Fig. 8. Fe–12Cr–1.5^{59}Ni specimen 735N irradiated at 400°C to 7.5 dpa and 77 appm He imaged using $\vec{g} = 110$ in (a), $\vec{g} = 002$ in (b) and void contrast in (c) for a foil near $(\bar{1}10)$ orientation.

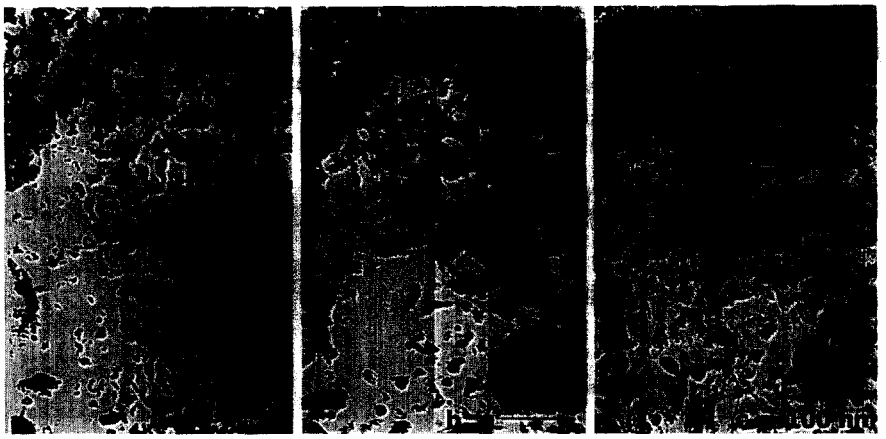

Fig. 9. Fe–12Cr–1.5^{Nat}Ni specimen 745N irradiated at 400°C to 7.4 dpa and 46 appm He imaged using $\vec{g} = 110$ in (a), $\vec{g} = 002$ in (b) and void contrast in (c) for a foil near $(\bar{1}10)$ orientation.

Precipitation, similar to the equiaxed phase found in 6A5N can be found but several examples of a rod shaped phase 7 nm wide and 24 nm long can be identified. Therefore major differences arising from the addition of ^{60}Ni are larger loops, smaller maximum void diameters and the presence of a rod shaped precipitate phase.

The microstructure of specimen 735N, Fe–12Cr–1.5^{59}Ni, following irradiation to about 7 dpa at 400°C and 76 appm He, was again found to exhibit differences. The dislocation structure was similar but precipitation appeared to be more advanced and cavitation could not be identified, suggesting that it was on a much finer scale. Examples are provided in Fig. 8. An area is shown in $\vec{g} = 110$ contrast (a), $\vec{g} = 002$ contrast (b) and void contrast (c) for a foil near a $(\bar{1}10)$ orientation. Loops 130 nm in diameter can be identified, and several short line segments can be found which may be remnants of even larger loops. However, the dominant microstructural features are precipitates, in the form of rod shaped features as large as 20 nm wide and 60 nm long. The microstructure is so complex that it is difficult to understand cavitation information, but if cavities are present, Fig. 8c indicates that they must be less than 2 nm in diameter. Therefore, it appears that additions of helium to levels on the order of 75 appm result in

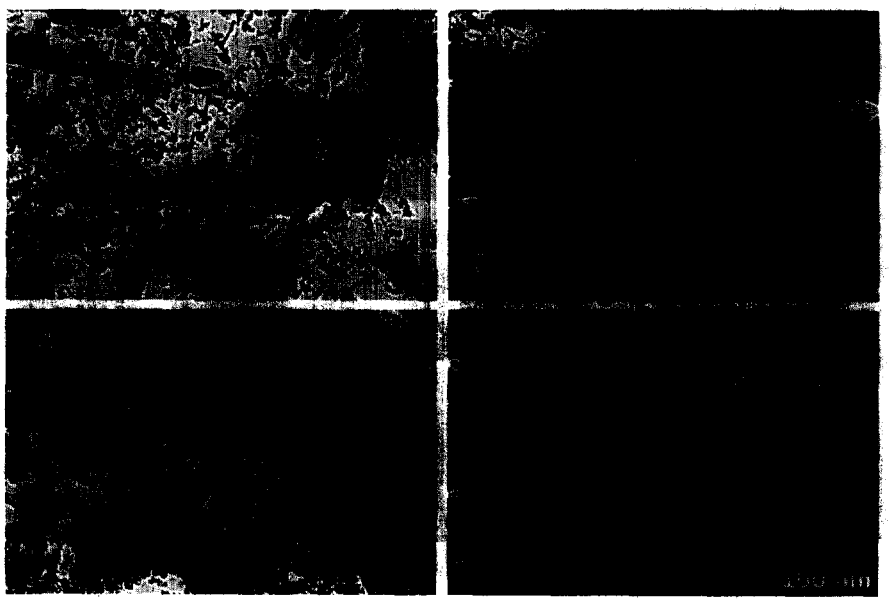

Fig. 10. Bright and dark field images of precipitation in Fe–12Cr–1.5^{60}Ni specimen 715N and Fe–12Cr–1.5^{59}Ni specimen 735N irradiated at 400°C to 7 dpa.

enhanced accumulation of interstitials to dislocation loops, enhanced precipitation kinetics, and most probably a much finer distribution of helium bubbles.

The microstructure of specimen 745N, Fe–12Cr–1.5^{Nat}Ni, following irradiation to 7 dpa at 400°C and 40 appm He was found to be similar, confirming conclusions obtained based on specimen 735N. Examples of the irradiated microstructure are shown in Fig. 9. Again, an area is

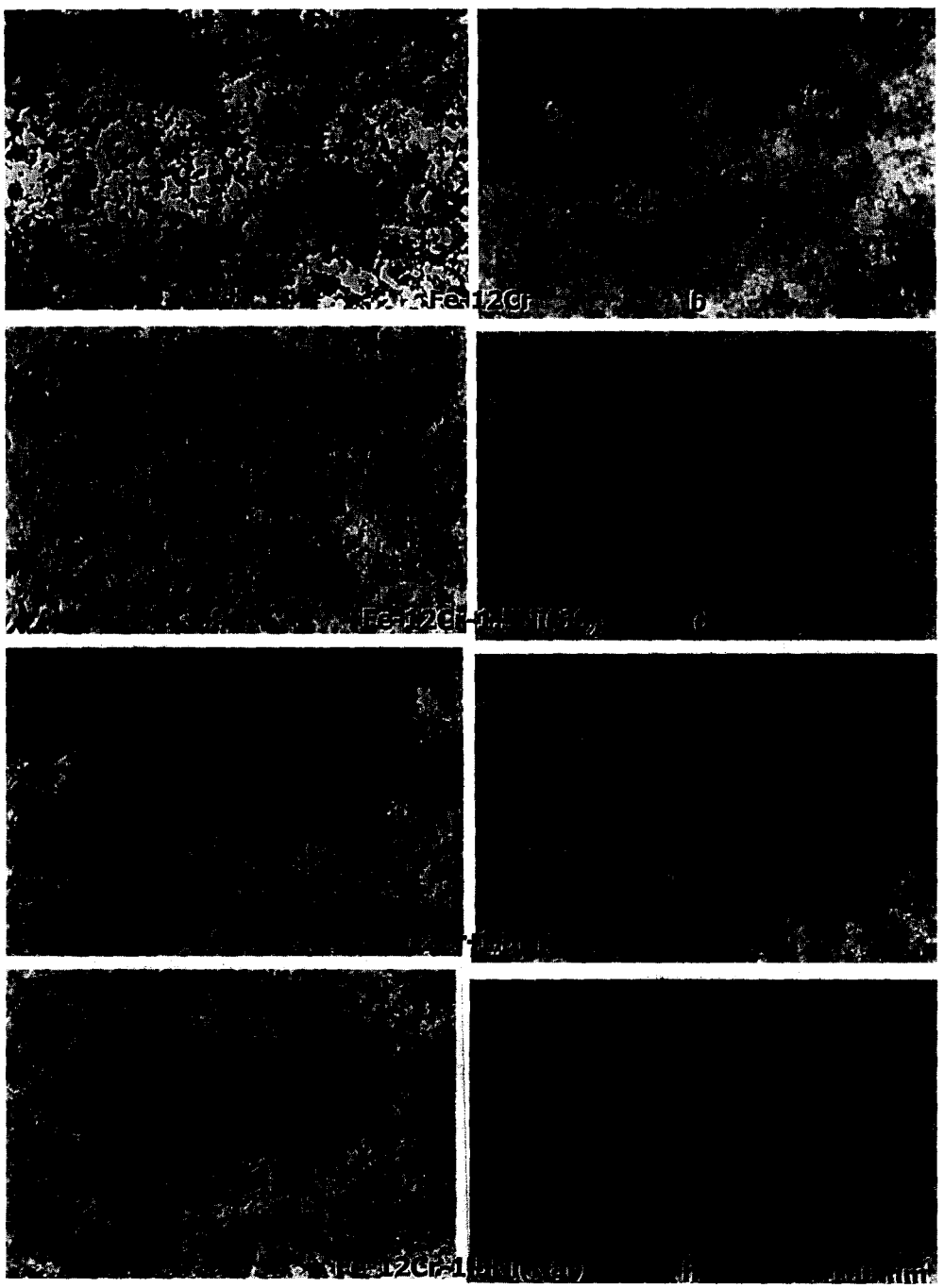

Fig. 11. A $\vec{g} = 110$ dislocation and void contrast image, respectively, for specimens irradiated at 300°C, (a) and (b) Fe–12Cr Specimen 6A5M Irradiated to 6.5 dpa and 2 appm He, (c) and (d) Fe–12Cr–1.5^{60}Ni specimen 715M irradiated to 6.4 dpa and 2 appm He, (e) and (f) Fe–12Cr–1.5^{59}Ni specimen 735M irradiated to 6.6 dpa and 71 appm He, and (g) and (h) Fe–12Cr–1.5^{Nat}Ni specimen 745M irradiated to 6.5 dpa and 41 appm He.

shown in $\vec{g} = 110$ contrast (a), $\vec{g} = 002$ contrast (b) and void contrast (c) for a foil near a $(\bar{1}10)$ orientation. Loops 200 nm in diameter can be identified, and several short line segments can be found which may be remnants of even larger loops. The dominant microstructural features are again precipitates, in the form of rod shaped features as large as 15 nm wide and 50 nm long. This microstructure is also so complex that it is difficult to understand cavitation information, but if cavities are present, they are less than 3 nm in diameter.

In order to further emphasize that nickel additions lead to precipitation Fig. 10 has been prepared showing precipitate dark field images in specimens 715N and 735N. In both cases, the precipitate dark field image was taken for an orientation near $(\bar{2}10)$ for $\vec{g} \approx \frac{2}{3}(420)$ and the bright field image was without further tilt. The areas chosen for publication include larger precipitate particles located on subgrain boundaries, in order to emphasize that particle growth was accelerated at boundaries. Although particle sizes for these two conditions appear to be similar based on the dark field images, the bright field images emphasize the greater complexity that appears to arise from the added helium. Certainly, it must be concluded that nickel additions to Fe–12Cr develop complex microstructures due to precipitation.

The microstructural developments found in specimens irradiated at 400°C are much more difficult to demonstrate in specimens irradiated at 300°C. The scale of the irradiation induced microstructure was finer and precipitation due to the presence of nickel appeared to be significantly reduced. Examples are provided in Fig. 11, showing each of the 300°C irradiation conditions in $\vec{g} = 110$ contrast (with the g → direction rotated 90° from previous figures), and void contrast for foils near (100) orientation. Of particular note is the fact that void-like features can be seen in Fig. 11d, f, h, indicating voids as large as 3 nm, but at much higher density in specimens 735M and 745M. Therefore, irradiation at 300°C appears to promote less precipitation than at 400°C.

4. Discussion

The experimental results of this ferritic/martensitic isotopic tailoring experiments require further discussion regarding the details of helium accumulation, and the consequences of both microstructural observations and mechanical properties.

4.1. Helium accumulation from isotopic tailoring

Additions of nickel isotopes to a base alloy have two well understood consequences. Not only can the amount of helium be varied by the two step transmutation reaction, but the actual accumulated displacement dose can be affected. Therefore, as various nickel additions are added to the base composition, Fe–12Cr, not only is the helium production varied, but also changes in dose arise. However, because the amount of nickel present in the alloys is low, the variation in dose from one specimen condition to another is also low, as shown from Table 1. In comparison, the helium production varies greatly from alloy to alloy. In both the base alloy and the alloy containing ^{60}Ni, helium is only produced from the presence of Fe and Cr. When ^{Nat}Ni is added, helium generation is not immediate and requires about 10 dpa to reach levels approaching steady state [2]. Therefore, in the Fe–12Cr–^{Nat}Ni alloy, helium production is non-linear, but approaches a steady state level by 7 dpa. In the Fe–12Cr–^{59}Ni alloy, helium production starts immediately and is approximately linear with dose, more representative of response in a fusion reactor.

4.2. Consequences of microstructural evolution

This helium accumulation response means that each of the alloys studied provides different insights into the radiation damage response in ferritic/martensitic alloys. Comparison of response in the base Fe–12Cr alloy with that in Fe–12Cr–^{60}Ni gives insight into the effect of nickel on response without variations in dose or helium production. Comparison of response in the Fe–12Cr–^{60}Ni alloy with that in the Fe–12Cr–^{59}Ni alloy shows effects of steady state helium production, 0.3 and 10 appm He/dpa, respectively. Lastly, comparison of response in the Fe–12Cr–^{59}Ni alloy with that in Fe–12Cr–^{Nat}Ni demonstrates the effect of non-linear helium additions with increasing dose.

The experimental results can be summarized as follows.

Nickel additions promote strength increases and precipitation in all alloys, but the strength increases are larger following irradiation at 300°C than at 400°C, whereas when no nickel is added, strengths are similar for the two irradiation temperatures. However, the cause of the additional strength for the 300°C could not be elucidated by microstructural examination, probably because the features were too small to be resolved.

There is sufficient dose by 7 dpa (and with 2 appm He) to initiate void swelling in ferritic/martensitic alloys.

Little difference was found between response from ^{59}Ni and ^{Nat}Ni additions, (perhaps in part because quantitative measurements are not complete), so that the rate of helium accumulation did not appear to affect microstructural evolution.

Helium bubble development for high helium generation conditions appeared to be very different at 300 and 400°C. At 300°C, it appeared that high densities of bubbles formed whereas at 400°C, bubbles could not be identified, possibly because of the complexity of the microstructure, but more likely because helium accumulated at precipitate interfaces. However, the bubble-like features found following irradiation at 300°C may have been associated with precipitates; no through focus imaging was attempted.

These results indicate that the addition of nickel isotopes to ferritic/martensitic steels in order to provide understanding of helium effects adds the complicating factor of precipitate formation in interpretation of response.

4.3. Consequences from mechanical property testing

It is clear from Figs. 1 and 2 that nickel additions significantly increase the τ_{sy} and τ_{sm} of the alloys before irradiation. The same is true following irradiation although the increase is less pronounced at higher temperatures, which suggests that the strengthening action was present at least in part, prior to irradiation. It may have arisen during the tempering heat treatment given the alloys of 760°C/1 h/air cool or may be due to solution strengthening due to the addition of nickel. The slight variability observed in the strength for each isotopic variation is currently unexplained, but may arise from variability in impurity levels associated with the isotopic additions. Irradiation at 300 and 400°C both caused an increase in strength when compared to the unirradiated material with the greatest strengthening occurring at 300°C. This is in agreement with the microstructural analysis carried on the same set of alloys. The microstructure of the material irradiated at 300°C exhibited a dense distribution of features. These features would be expected to produce an increase in the strength of the alloy. The material irradiated at 400°C showed a more coarse microstructure, with larger and fewer precipitates and fewer, but more developed, dislocation loops. The material irradiated at 500 and 600°C showed an overall reduction in strength when compared with the unirradiated condition. Although the microstructures have not been studied for the alloys irradiated at 500 and 600°C, it is expected that further coarsening and increased loop and precipitate growth will have occurred. [16]

The plot of $\Delta\tau_{sy}$ versus helium content (Fig. 3) shows a shallow positive gradient for materials irradiated at the lower temperatures. This trend is reversed, but has a slightly steeper gradient, in the plot of $\Delta\tau_{sm}$ versus helium level (Fig. 4). The variation in $\Delta\tau_{sy}$ over the range of helium levels for irradiation at a given temperature is only about 30 MPa, which is essentially the same as the scatter in the data for a given test condition (± 20 MPa). It is therefore difficult to draw any conclusions, other than that helium levels up to 75 appm have little or no influence on the mechanical properties over the range of temperatures considered.

5. Conclusions

Isotopic tailoring by additions of 1.5% nickel of ^{60}Ni, ^{59}Ni, and ^{Nat}Ni to a base alloy Fe–12Cr have provided ferritic/martensitic alloys with very different helium levels following irradiation in the HFIR to 7 dpa at 300 to 600°C. Shear punch tests showed that helium levels up to 75 appm have little, if any, effect on the effective shear yield and maximum shear strengths. The strengthening effect of nickel was evident prior to irradiation and the strength of the irradiated Fe–12Cr–1.5Ni ferritic alloys shows a strong dependence on irradiation temperature, decreasing with increasing irradiation temperature.

Microstructural examinations revealed: (1) Nickel additions promote precipitation in all alloys, but the effect appears to be much stronger at 400°C than at 300°C. (2) There is sufficient dose by 7 dpa (and with 2 appm He) to initiate void swelling in ferritic/martensitic alloys. (3) Little difference was found between response from ^{59}Ni and ^{Nat}Ni, indicating that a change in the rate of helium production did not affect microstructure. (4) Helium bubble development for high helium generation conditions appeared to be very different at 300 and 400°C. At 300°C, it appeared that high densities of void-like features formed, whereas at 400°C, bubbles could not be identified, possibly because of the complexity of the microstructure, but more likely because helium accumulated at precipitate interfaces.

Future studies on helium effects in ferritic/martensitic steels should not be based on nickel additions because large microstructural changes arise from nickel precipitation making comparison with typical ferritic/martensitic steels unrealistic.

Conclusions from previous experiments should be reevaluated.

Acknowledgements

Many have played a role allowing this experiment to reach fruition: to R.L. Simon, who first proposed the idea, with encouragement from G.R. Odette; to F.A. Garner who made the ^{59}Ni available for this project and encouraged in many other ways, to P.J. Maziasz who made the ^{60}Ni available and built the first HFIR irradiation experiments, to R.M. Ermi who melted the alloys, to E.M. Dieffenbacher who prepared specimens, to A.E. Ermi who organized the JP23 experiment, to J.E. Pawels, who built the JP23 experiment and distributed specimens, to A.F. Rowcliffe who fathered this experiment from its inception and to its completion, to E.M. Dieffenbacher and B.A. Walker who thinned the specimens for examinations, to E.M. Dieffenbacher who transferred the specimens for shear punch testing and finally to L.R. Greenwood who provided further understanding of the transmutation response. This work was supported in part by the US Department of Energy under Contract DE-AC06-76RLO 1830.

References

[1] R.L. Simon, Damage Analysis and Fundamental Studies Quarterly Progress Report, Oct.–Dec. 1982, DOE/ER-0046/12, 1983, p. 37.

[2] G.R. Odette, J. Nucl. Mater. 141–143 (1986) 1011.
[3] F.A. Garner, M.L. Hamilton, R.L. Simon, M.K. Maxon, J. Nucl. Mater. 179–181 (1991) 554.
[4] M.L. Hamilton, F.A. Garner, J. Nucl. Mater. 191–194 (1992) 1239.
[5] M.L. Hamilton, F.A. Garner, D.J. Edwards, J. Nucl. Mater. 212–215 (1994) 325.
[6] D.S. Gelles, J. Nucl. Mater. 108&109 (1982) 515.
[7] D.S. Gelles, R.L. Meinecke, Alloy Development for Irradiation Performance Progress Report for Period Ending September 1983, DOE/ER-0045/11, 1984, p. 103.
[8] R.L. Simon, H.R. Brager, W.Y. Matsumoto, J. Nucl. Mater. 141–143 (1986) 1057.
[9] D.S. Gelles, in: Effects of Radiation on Materials: 14th Int. Symp., Vol. 1, ASTM STP 1046, eds. N.H. Packan, R.E. Stoller and A.S. Kumar (American Society for Testing and Materials, Philadelphia, PA, 1989) p. 73.
[10] Y. Katoh, A. Kohyama, D.S. Gelles, J. Nucl. Mater. 225 (1995) 154.
[11] D.S. Gelles, J. Nucl. Mater. 225 (1995) 163.
[12] A.M. Ermi, D.S. Gelles, Fusion Materials Semiannual Progress Report for the Period Ending September 30, 1994, DOE/ER-0313/17, p. 35.
[13] L.R. Greenwood, R.T. Ratner, Fusion Materials Semiannual Progress Report for the Period Ending June 30, 1996, DOE/ER-0313/20, p. 305.
[14] M.L. Hamilton, M.B. Toloczko, G.E. Lucas, in: Miniaturized Specimens for Testing of Irradiated Materials, eds. H. Ullmaier and P. Jung (Forschungszentrum Jülich, Jülich, Jan. 1995) p. 46.
[15] G.E. Lucas, G.R. Odette, J.W., Sheckherd, The Use of Small Scale Specimens for Testing Irradiated Material, ASTM STP 888 (American Society for Testing and Materials, Philadelphia, PA, 1986) p. 112.
[16] M.L. Hamilton, M.B. Toloczko, D.J. Edwards, W.F. Sommer, M.J. Borden, J.A. Dunlap, J.F. Stubbins, G.E. Lucas, in: Effects of Radiation on Materials: 17th Int. Symp., ASTM STP 1270, eds. D.S. Gelles, R.K. Nanstad, A.S. Kumar and E.S. Little (American Society for Testing and Materials, Philadelphia, PA, 1996) p. 1057.
[17] M.B. Toloczko, M.L. Hamilton, G.E. Lucas, 'Ductility correlations between shear punch and uniaxial tensile data', submitted to J. Nucl. Mater.
[18] D.S. Gelles, L.E. Thomas, in: Proc. Topical Conf. on Ferritic Alloys for Use in Nuclear Energy Technologies, eds. J.W. Davis and D.J. Michel (AIME, Warrendale, PA, 1984) p. 559.